Biochemical and Biophysical Research Communications 550 (2021) 191–196

Contents lists available at ScienceDirect

Biochemical and Biophysical Research Communications

journal homepage: www.elsevier.com/locate/ybbrc

Beta-strand-mediated dimeric formation of the Ig-like domains of human lamin A/C and B1

Jinsook Ahn [a], Jinwook Lee [a], Soyeon Jeong [a], So-mi Kang [b], Bum-Joon Park [b], Nam-Chul Ha [a, *]

[a] Department of Agricultural Biotechnology, Centre for Food Safety and Toxicology, Centre for Food and Bioconvergence, Research Institute for Agriculture and Life Sciences, CALS, Seoul National University, Seoul, 08826, Republic of Korea
[b] Department of Molecular Biology, College of Natural Science, Pusan National University, Busan, 46241, Republic of Korea

ARTICLE INFO

Article history:
Received 18 February 2021
Accepted 22 February 2021
Available online 9 March 2021

Keywords:
Lamin A/C
Lamin B1
Ig-like domain
Crystal structure
Dimeric assembly
Lamin filament

ABSTRACT

Lamins are nuclear intermediate filament proteins that play an essential role in maintaining the nuclear structure by forming a 3-D meshwork. Lamins consist of the N-terminal unstructured head, the coiled-coil rod domain, and the C-terminal tail, which is mostly unstructured except for the Ig-like domain. To date, the Ig-like domain has been characterized as a monomeric structure. Here, we determined the crystal structures of human lamin A/C, including the Ig-like domain and its N- and C-terminal flanking sequences. Interestingly, the structures showed a homodimer formed by beta-strand interactions between the N- and C-terminal flanking sequences. This interaction also provides a molecular implication for the creation of a 3-D meshwork between the 3.5-nm-thick filaments. Furthermore, we determined the crystal structure of the corresponding region of lamin B1. The structure showed a similar dimeric assembly, also formed by beta-strand interactions, albeit the intersubunit distance was much shorter. Since the Ig-like domain contains many genetic hotspots causing lamin-related diseases in lamin A/C, our findings will help understand the detailed assembly of lamins in a 3-D meshwork structure and lamin-related diseases at the molecular level.

1. Introduction

Intermediate filaments (IFs), mostly consisting of alpha-helical coiled-coil, provide mechanical support in the diverse subcellular regions of eukaryotic cells. In the nucleus IF lamins, together with lamin-binding proteins, play essential roles in maintaining the nuclear architecture and supporting chromosomes with several nuclear functions [1,2]. Many mutations in lamin genes are related to human genetic disorders, including progeroid syndromes, Emery-Dreifuss muscular dystrophy (EDMD), and Dunnigan-type lipodystrophy [3–7]. The lamin structure and function are critical in developing drugs against lamin-related diseases and in understanding the fundamentals of life phenomena, including the human aging process.

Lamins consist of the N-terminal unstructured head, the alpha-helical central coiled-coil rod domain, and C-terminal tail. The central alpha-helical rod domain forms a long parallel homodimer as the fundamental building block in the soluble state. The N-terminal head and C-terminal tail regions are mainly unstructured except for the globular Ig-like domain in the C-terminal tail [8,9]. Lamin A/C is differentially expressed depending on the tissue type, whereas lamin B1 is constitutively expressed in most cell types in humans [10]. Confocal microscopy studies revealed that lamin A/C and lamin B1 form separate meshworks in HeLa cell nuclei [11].

The crystal structure of a long fragment of the central rod domain of lamin A/C revealed the tetrameric unit of two dimers, formed by the so-called A11 interaction. The structures further proposed an assembly mechanism, where the longitudinal assembly between the tetrameric units is formed by the so-called eA22 interaction [12–14]. According to Ahn's model, subsequent and alternating A11 and eA22 interactions induced long linear filamentous oligomers with a thickness of 3.5 nm, explaining the *in situ* cryo-electron tomographic (cryo-ET) images at the molecular and pseudomolecular levels [15,16]. Moreover, the cryo-ET images suggested that the multiple 3.5-nm-thick linear filaments are entangled to form the 3-D meshwork. The final 3-D model of lamin is different from those of cytosolic members of intermediate

* Corresponding author.
E-mail address: hanc210@snu.ac.kr (N.-C. Ha).

https://doi.org/10.1016/j.bbrc.2021.02.102
0006-291X/

filaments, formed by the side-by-side bundling of the 3.5-nm-thick linear filaments or their equivalent linear units.

NMR spectroscopy and X-ray crystallography have structurally characterized the fragments of lamin A/C covering the Ig-like domain, showing substantially the same structural features in their protomers [4,9]. In solution, a dimeric form was suggested by SDS-PAGE analysis [17]. The Ig-like domain of human lamin A adopts an Ig-like fold, containing hot spot mutations that cause many genetic disorders [4,6,18,19]. However, since the structures represent only a short fragment of the Ig-like domain, the roles of the Ig-like domain in the full-length context still have ambiguities. This study determined the crystal structures of the Ig-like domains of lamin A/C and lamin B1, including the N- and C-terminal flanking sequences. The structures implicate the dimeric assembly of the Ig-like domains in the cell, proposing critical roles in forming the 3-D meshwork structure of the lamins.

2. Materials and methods

2.1. Plasmid construction

For overexpression of lamin proteins, DNA encoding human lamin A/C 406–552 and lamin B1 407–553 were PCR-amplified from human full-length lamin A/C and B1, respectively [26]. To clone lamin A/C (residues 406–552), primers (forward, 5′-GGCGAATTCTCATCCCAGACACAGGGTG-3'; reverse, 5′-GCCAAGCTTTTAGTCCTCAACCACAGTCAC-3′) were used. For the lamin B1 construct, primers (forward, 5′-GCGGAATTCCGTAGTG-TACGTACAACTAG; reverse, 5′-GCGAAGCTT TCATTCTTCAGG-TATGGTTG-3′) were used. The amplified DNA molecules were inserted into the EcoRI and HindIII sites of the pProEx-HTa vector (Thermo Fisher Scientific, MA, USA). The plasmid construction for the lamin A/C (residues 301–565) fragment was described previously [26].

2.2. Purification of the recombinant proteins

Each plasmid encoding the lamin A/C and lamin B1 fragments was transformed into *E. coli* BL21 (DE3) (Novagen, USA) and cultured in LB or terrific broth medium. Protein expression was induced by 0.5 mM IPTG at 30 °C. The cells were harvested by centrifugation and resuspended in lysis buffer containing 20 mM Tris-HCl (pH 8.0) and 150 mM NaCl. The cells were disrupted by sonication, and then the cell debris was removed by precipitation via centrifugation at 13,000 rpm. The supernatant was loaded onto TALON® superflow™ metal affinity resin (GE Healthcare, California, USA) and preincubated with lysis buffer. The target protein was eluted with lysis buffer supplemented with 250 mM imidazole. The protein was treated with recombinant TEV protease to cleave the His-tag and then loaded onto a HiTrap Q-column (GE Healthcare, California, USA), and a linear gradient of increasing NaCl concentration was applied to the HiTrap Q column. The fractions which contained the protein were applied onto a size exclusion chromatography column (HiLoad Superdex 200 26/600 column; GE Healthcare, California, USA), pre-equilibrated with lysis buffer. The purified protein in lysis buffer was concentrated to 15 mg/mL and frozen at −70 °C.

2.3. Crystallization and structure determination

Extended Ig-like domain of lamin A/C protein (15 mg/ml), whose hexa His-tag was cleaved off, was crystallized in a precipitation solution containing 0.2 M potassium chloride, 0.05 M HEPES pH 7.5, and pentaerythritol propoxylate (5/4 PO/OH) using the hanging-drop vapor diffusion method at 16 °C. The lamin B1 e-Ig domain protein (7.5 mg/ml) was crystallized in 0.2 M magnesium nitrate (pH 5.9) and 20% (w/v) polyethylene glycol (molecular weight 3350) using the hanging-drop vapor diffusion method at 16 °C. The crystals of lamin A/C were briefly soaked in a cryoprotectant solution containing 25% glycerol, and the lamin B1 crystals were transferred to the viscous oil Paraton-N. Then, the crystals were flash-frozen in a liquid nitrogen stream at −173 °C. The diffraction datasets were collected at Accelerator Laboratory Beamline 5C using an Eiger 9 M detector and were processed with the HKL2000 package [27].

The structure of the extended Ig-like domains was determined using the molecular replacement method with MOLREP in the CCP4 package [28]. The crystals of the lamin A/C e-Ig domain belong to space group $P6_422$ with unit-cell dimensions of $a = 92.6$ Å, $b = 92.6$ Å, and $c = 206.0$ Å. The lamin B1 e-Ig domain crystals belong to the space group $C222_1$ with unit-cell dimensions of $a = 144.6$ Å, $b = 160.7$ Å, and $c = 132.8$ Å (Supplementary Table 1). The programs COOT and PHENIX were used for model building and refinement [29–32]. Statistical information regarding data collection and processing is presented in Supplementary Table 1.

3. Results

3.1. Stable fragments containing the Ig-like domain of human lamin A/C and its flanking sequence

To expand the structural information of the Ig-like domain, we expressed a longer construct (residues 301–565), including the Ig-like domain of human lamin A/C, than the Ig-like domain previously structurally characterized (residues 428–549; Fig. 1A). The fragment was easily degraded into three shorter pieces containing the Ig-like domain during the purification step (Fig. 1B). Size exclusion chromatography segregated the degradation products based on their molecular sizes (Fig. 1B). The N-terminal sequencing analysis of the most compact fragments identified that the fragment consists of residues 406–552. The fragment was named an extended Ig-like domain (hereafter called the e-Ig domain) because it contained the Ig-like domain and its N- and C-terminal flanking sequences (406–428 and 549–552). Size exclusion chromatography combined with multiangle light scattering (SEC-MALS) revealed that the e-Ig domain behaved as a monomer in solution (Supplementary Fig. 1).

3.2. The dimeric form of the lamin A/C e-Ig domain

Next, we determined the crystal structures of the lamin A/C e-Ig domain with the stable fragment at 1.8 Å resolution in the $P6_422$ space group (Supplementary Table 1). The asymmetric unit in the crystal contained three molecules (Supplementary Fig. 2A). The overall structure of the monomer is similar to the Ig-like domain structures previously determined [4,9] (Fig. 2A and Supplementary Fig. 3). Structural superpositions with the previously determined structures of the Ig-like domains [4,9] revealed that the Ig-like fold is shared, including the N- and C-terminal paired beta-strands in an antiparallel manner (Supplementary Fig. 3). However, the paired beta-strands of the N- and C-terminal regions in the e-Ig domain were much longer than those of only the Ig-like domain part [9] (Fig. 2B and Supplementary Fig. 3).

The crystal structures showed that the N- and C-terminal flanking sequences in the paired beta-strands are in the dimeric interface, resulting in a long, four-stranded beta-sheet (Fig. 2B). Beta-stranded dimeric interactions are formed by hydrogen bonds between the backbone carboxyl and amide bonds without any interaction between the side chains. Since the amino acid sequence in the dimeric interface is mostly hydrophilic, this interaction

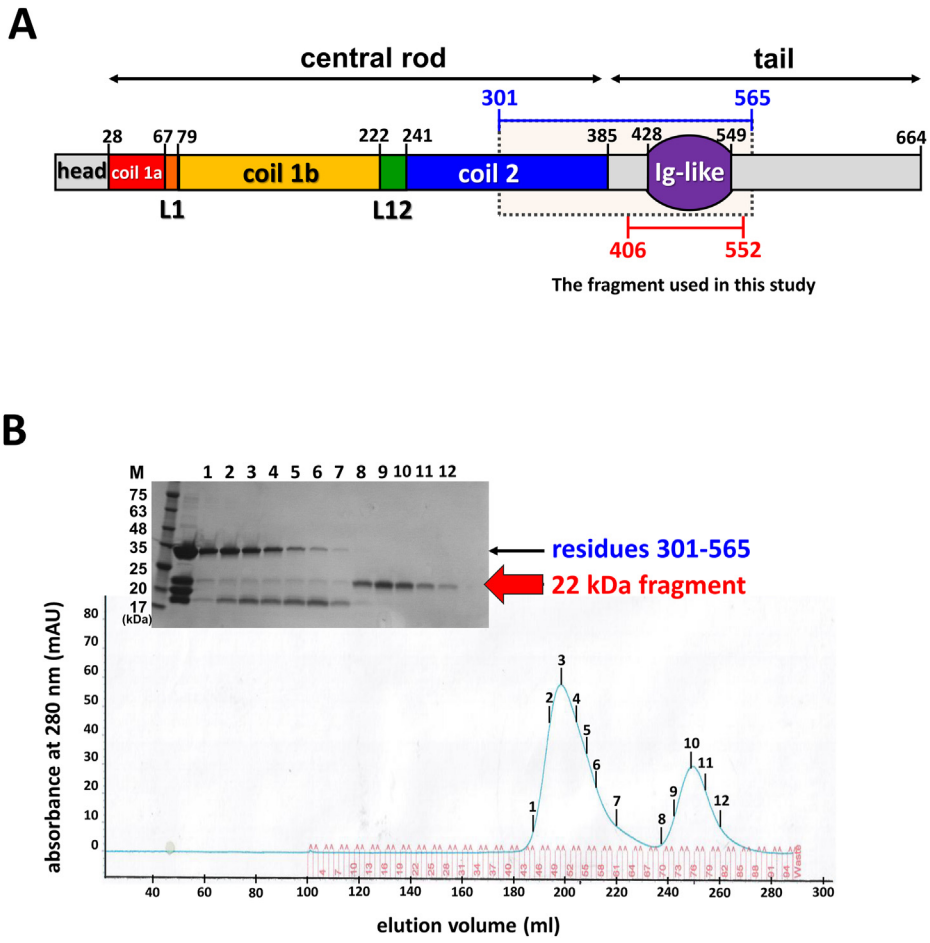

Fig. 1. The construct of the extended Ig-like domain (e-Ig domain) of human lamin A/C.
(A) Schematic domain organization of lamin A, consisting of the head, central rod, and tail region. The central rod domain is further divided into coil 1a, L1, coil 1b, L12, and coil 2. The tail domain contains the Ig-like domain. The longer construct containing the Ig-like domain (residues 301–565) and the e-Ig domain for the structural study (residues 406–552) are indicated.
(B) SDS-polyacrylamide gel showing the fractions of the size exclusion chromatography with the degradation products from the longer construct (residues 301–565). The 22-kDa protein band (e-Ig domain), indicated by the red arrow, was subjected to Edman degradation for determination of the N-terminal residues. The size markers (M) are labeled on the left. (For interpretation of the references to colour in this figure legend, the reader is referred to the Web version of this article.)

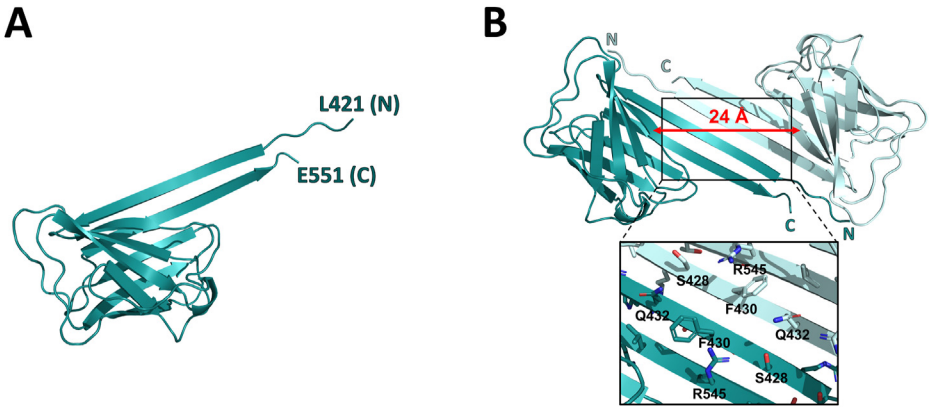

Fig. 2. The crystal structure of the extended Ig-like domain of lamin A/C.
(A) The overall structure of the e-Ig domain in lamin A/C. The conventional Ig-like domain and the flanking sequences are indicated. The N- and C-terminal residues are marked. (B) The dimeric arrangement of the two protomers in the asymmetric unit. The dimeric interface consisting of the flanking sequences is enlarged in the bottom panel. The distance between the e-Ig domain, based on the Glu 444 residues, is represented by a double-headed red arrow. (For interpretation of the references to colour in this figure legend, the reader is referred to the Web version of this article.)

appears weak and reversible. Due to this long, four-stranded beta-sheet, the main Ig-like domains are separated by 24 Å in this dimeric assembly. Since Phe430 is in the center of the dimeric interface, the Phe430 residues are closest to the dimeric structure (Fig. 2B).

3.3. The crystal structure of the lamin B1 e-Ig domain

Crystal structures of the lamin B1 Ig-like domain are available [20]. However, none of the constructs used for the structural studies contained flanking sequences around the Ig-like domain. To examine whether the e-Ig domain of lamin B1 has a dimeric propensity, we produced the corresponding fragment of the e-Ig domain of lamin B1 by sequence comparison to lamin A/C. The e-Ig domain fragment of lamin B1 (residues 407–553) was well expressed in the *E. coli* expression system. We determined the crystal structure of the e-Ig domain of lamin B1 at 3.6 Å resolution using the Ig-like domain of lamin B1 (PDB ID: 3UMN) as the search model for the molecular replacement method (Fig. 3) [20].

The crystal structure of the lamin B1 e-Ig domain was virtually the same as the Ig-like domain structures of lamin B1 that were previously determined [20] (Supplementary Fig. 4). All the lamin B1 Ig-like domain structures, including this lamin B1 e-Ig domain structure, revealed a similar putative dimeric interface mediated by the beta-strand interaction between the backbone atoms. These findings show that the Ig-like domains have a propensity to form a dimer, although the flanking sequence of the Ig-like domain of lamin B1 did not participate in the dimerization. The distance between the protomers of the lamin B1 Ig-like domains is 8.4 Å, which is shorter than that of the lamin A/C e-Ig domains (Fig. 3). The Ig-like domains are slipped toward the center of the dimer by nine residues (~28 Å) compared with the lamin A/C e-Ig domains (Fig. 4).

4. Discussion

Here, we determined the crystal structures of the Ig-like domains, including the flanking sequences, of lamin A/C and lamin B1. The Ig-like domain of lamin A/C showed a long beta-strand interaction between the protomers in the dimeric assembly. Lamin B1 exhibited a shorter dimeric interface consisting of a shorter paired beta-strand interaction than that of the lamin A/C Ig-like domain.

Size exclusion chromatography showed that the e-Ig domain proteins of lamin A/C and lamin B1 did not make dimeric assemblies in the solution (Supplementary Fig. 1). These results indicate that the dimeric propensity of the e-Ig domain might not be strong enough to contribute to the formation of the 3.5-nm linear filament. Lamin proteins require multiple hierarchical interactions between the lamin protomers to form the final 3-D meshwork [12–14,21]. We believe that dimerization between the e-Ig domain should become important above the steps of 3.5-nm-thick filament formation in the cells.

How would the weak dimeric assembly of the Ig-like domain be enhanced in the full-length lamin protein in cells? First, we noted the multivalent Ig-like domains alongside the central 3.5-nm filament. Thus, the structural model, including the Ig-like domains, is reminiscent of a centipede, in which the body is the central filament, and the feet are the Ig-like domains. If the two filaments were arranged side-by-side, the numerous Ig domains would immediately become closer because the pitches between the Ig domains are all the same. This geometrical arrangement would amplify the interaction between the Ig-like domains from each filament, like molecular Velcro. These Velcro-like interactions could be more enhanced in the 3-D meshwork structures because of the higher density of the e-Ig domains in the meshwork structure. Second, the Ig-like domain of lamin A/C is tethered to the chromosome and nuclear membranes via the barrier-to-autointegration factor (BAF) [22–24]. These binding partners might provide another attaching point between the adjacent Ig domains.

The *in situ* cryo-ET structure should be considered a blueprint for the final lamin meshwork to solve these puzzles [15,25]. The cryo-ET image showed bulbs representing the dimeric assembly of the Ig-like domain in the space between the 3.5-nm-thick filaments. Based on these observations, we propose a higher-order assembly of the lamins, where the Ig-like domains provide contact surfaces between the filaments (Supplementary Fig. 5).

The nuclear membrane should acquire both rigidity and flexibility. According to the cryo-ET images of the lamin, the 3.5-nm filaments are located in parallel [15,25]. We believe this

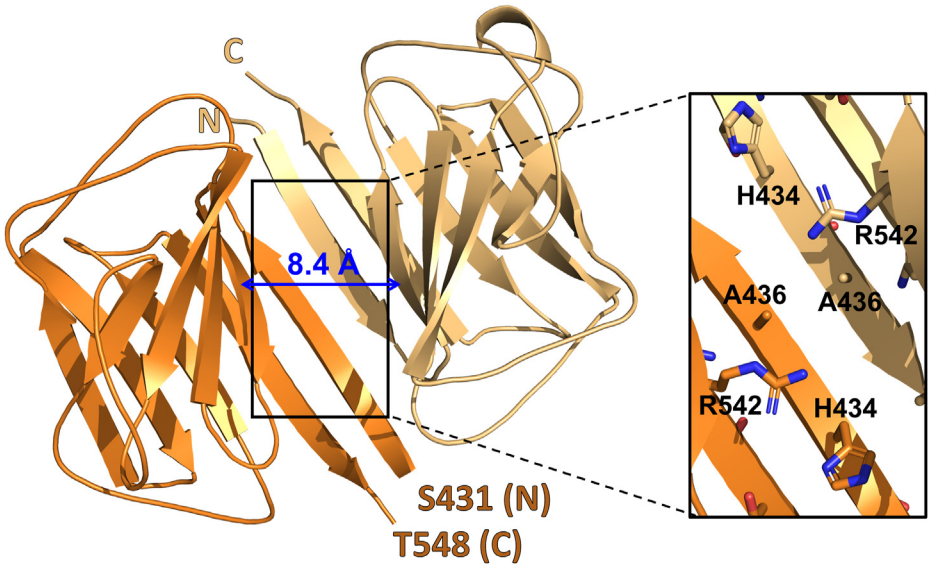

Fig. 3. The dimeric unit of the lamin B1 extended Ig-like domain observed in the crystal. The N- and C-terminal residues are marked. The distance between the e-Ig domain, based on the Glu 445 residues, is represented by a double-headed blue arrow. The dimeric interface is enlarged in the inset. (For interpretation of the references to colour in this figure legend, the reader is referred to the Web version of this article.)

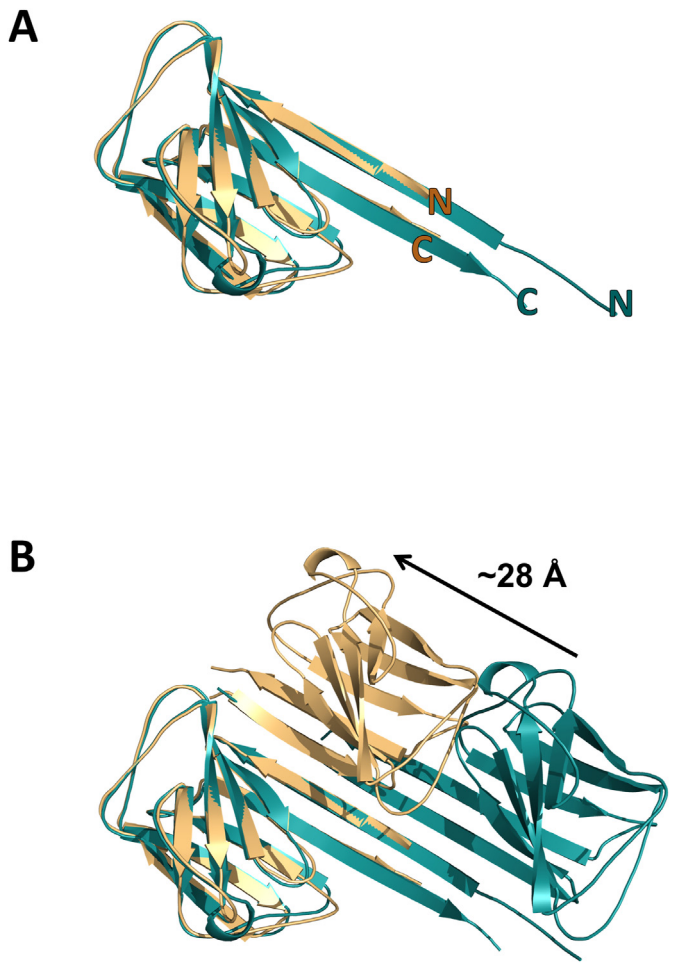

Fig. 4. Structural comparison of the extended Ig-like domains between lamin A/C (green) and lamin B1 (yellow).
(A) The structural superposition of a protomer of the e-Ig domain between lamin A/C and lamin B1.
(B) The structural superposition of the dimeric units of the e-Ig domains between lamin A/C and lamin B1. The black arrow indicates the slipped distance of the e-Ig domain between lamin A/C and lamin B1. (For interpretation of the references to colour in this figure legend, the reader is referred to the Web version of this article.)

arrangement between the filaments is critical for maintaining the physical properties of the nuclear lamina. In the case of the improper 3-D meshwork structure, the nuclear structure would be weakened to physical stresses or would decrease normal nuclear functions, resulting in cellular aging. Our findings will aid in understanding the detailed assembly of lamins in the 3-D meshwork structure and lamin-related diseases at the molecular level.

Declaration of competing interest

The authors declare that they have no known competing financial interests or personal relationships that could have appeared to influence the work reported in this paper.

Acknowledgments

This work was supported by grants from the National Research Foundation of Korea (2019R1A2C208513512). This research was supported by the Basic Research Program through the National Research Foundation of Korea (2020R1A4A101932211). We made use of beamline 5C at the Pohang Accelerator Laboratory (Pohang, Republic of Korea) and the MALS facility at the Korea Basic Science Institute (Ochang, Republic of Korea).

Appendix A. Supplementary data

Supplementary data to this article can be found online at https://doi.org/10.1016/j.bbrc.2021.02.102.

References

[1] K.L. Wilson, R. Foisner, Lamin-binding proteins, Cold Spring Harb. Perspect. Biol. 2 (2010) a000554, https://doi.org/10.1101/cshperspect.a000554.
[2] J. Gotzmann, R. Foisner, Lamins and lamin-binding proteins in functional chromatin organization, Crit. Rev. Eukaryot. Gene Expr. 9 (1999) 257–265, https://doi.org/10.1615/critreveukargeneexpr.v9.i3-4.100.
[3] B. Burke, C.L. Stewart, Life at the edge: the nuclear envelope and human disease, Nat. Rev. Mol. Cell Biol. 3 (2002) 575–585.
[4] E. Magracheva, S. Kozlov, C.L. Stewart, A. Wlodawer, A. Zdanov, Structure of the lamin A/C R482W mutant responsible for dominant familial partial lipodystrophy (FPLD), Acta Crystallogr. Sect. F Struct. Biol. Cryst. Commun. 65 (2009) 665–670, https://doi.org/10.1107/S1744309109020302.
[5] J. Scharner, H.C. Lu, F. Fraternali, J.A. Ellis, P.S. Zammit, Mapping disease-related missense mutations in the immunoglobulin-like fold domain of lamin A/C reveals novel genotype-phenotype associations for laminopathies, Proteins 82 (2014) 904–915, https://doi.org/10.1002/prot.24465.
[6] D.K. Shumaker, R.I. Lopez-Soler, S.A. Adam, H. Herrmann, R.D. Moir, T.P. Spann, R.D. Goldman, Functions and dysfunctions of the nuclear lamin Ig-fold domain in nuclear assembly, growth, and Emery-Dreifuss muscular dystrophy, Proc. Natl. Acad. Sci. U. S. A. 102 (2005) 15494–15499, https://doi.org/10.1073/pnas.0507612102.
[7] J. Ahn, T.-G. Woo, S.-m. Kang, I. Jo, J.-S. Woo, B.-J. Park, N.-C. Ha, The flavonoid morin alleviates nuclear deformation in aged cells by disrupting progerin-lamin A/C binding, J. Funct. Foods 77 104331.
[8] E. Heitlinger, M. Peter, A. Lustig, W. Villiger, E.A. Nigg, U. Aebi, The role of the head and tail domain in lamin structure and assembly: analysis of bacterially expressed chicken lamin A and truncated B2 lamins, J. Struct. Biol. 108 (1992) 74–89, https://doi.org/10.1016/1047-8477(92)90009-y.
[9] S. Dhe-Paganon, E.D. Werner, Y.I. Chi, S.E. Shoelson, Structure of the globular tail of nuclear lamin, J. Biol. Chem. 277 (2002) 17381–17384, https://doi.org/10.1074/jbc.C200038200.
[10] C. Stewart, B. Burke, Teratocarcinoma stem cells and early mouse embryos contain only a single major lamin polypeptide closely resembling lamin B, Cell 51 (1987) 383–392, https://doi.org/10.1016/0092-8674(87)90634-9.
[11] T. Shimi, K. Pfleghaar, S. Kojima, C.G. Pack, I. Solovei, A.E. Goldman, S.A. Adam, D.K. Shumaker, M. Kinjo, T. Cremer, R.D. Goldman, The A- and B-type nuclear lamin networks: microdomains involved in chromatin organization and transcription, Genes Dev. 22 (2008) 3409–3421, https://doi.org/10.1101/gad.1735208.
[12] J. Ahn, I. Jo, S.M. Kang, S. Hong, S. Kim, S. Jeong, Y.H. Kim, B.J. Park, N.C. Ha, Structural basis for lamin assembly at the molecular level, Nat. Commun. 10 (2019) 3757, https://doi.org/10.1038/s41467-019-11684-x.
[13] J. Ahn, S. Jeong, S.M. Kang, I. Jo, B.J. Park, N.C. Ha, Separation of coiled-coil structures in lamin A/C is required for the elongation of the filament, Cells 10 (2020), https://doi.org/10.3390/cells10010055.
[14] A.V. Lilina, A.A. Chernyatina, D. Guzenko, S.V. Strelkov, Lateral A11 type tetramerization in lamins, J. Struct. Biol. 209 (2020) 107404, https://doi.org/10.1016/j.jsb.2019.10.006.
[15] Y. Turgay, M. Eibauer, A.E. Goldman, T. Shimi, M. Khayat, K. Ben-Harush, A. Dubrovsky-Gaupp, K.T. Sapra, R.D. Goldman, O. Medalia, The molecular architecture of lamins in somatic cells, Nature 543 (2017) 261–264, https://doi.org/10.1038/nature21382.
[16] R. Tenga, O. Medalia, Structure and unique mechanical aspects of nuclear lamin filaments, Curr. Opin. Struct. Biol. 64 (2020) 152–159, https://doi.org/10.1016/j.sbi.2020.06.017.
[17] V. Stierlé, J. Couprie, C. Östlund, I. Krimm, S. Zinn-Justin, P. Hossenlopp, H.J. Worman, J.-C. Courvalin, I. Duband-Goulet, The carboxyl-terminal region common to lamins A and C contains a DNA binding domain, Biochemistry 42 (2003) 4819–4828.
[18] V.L. Verstraeten, S. Caputo, M.A. Van Steensel, I. Duband-Goulet, S. Zinn-Justin, M. Kamps, H.J. Kuijpers, C. Östlund, H.J. Worman, J.J. Briedé, The R439C mutation in LMNA causes lamin oligomerization and susceptibility to oxidative stress, J. Cell Mol. Med. 13 (2009) 959–971.
[19] I. Holt, C. Östlund, C.L. Stewart, N. thi Man, H.J. Worman, G.E. Morris, Effect of pathogenic mis-sense mutations in lamin A on its interaction with emerin in vivo, J. Cell Sci. 116 (2003) 3027–3035.
[20] J. Ruan, C. Xu, C. Bian, R. Lam, J.P. Wang, J. Kania, J. Min, J. Zang, Crystal structures of the coil 2B fragment and the globular tail domain of human lamin B1, FEBS Lett. 586 (2012) 314–318, https://doi.org/10.1016/j.febslet.2012.01.007.
[21] L.E. Kapinos, P. Burkhard, H. Herrmann, U. Aebi, S.V. Strelkov, Simultaneous formation of right- and left-handed anti-parallel coiled-coil interfaces by a coil2 fragment of human lamin A, J. Mol. Biol. 408 (2011) 135–146, https://

doi.org/10.1016/j.jmb.2011.02.037.
[22] C. Capanni, V. Cenni, T. Haraguchi, S. Squarzoni, S. Schuchner, E. Ogris, G. Novelli, N. Maraldi, G. Lattanzi, Lamin A precursor induces barrier-to-autointegration factor nuclear localization, Cell Cycle 9 (2010) 2600–2610, https://doi.org/10.4161/cc.9.13.12080.
[23] A. Mattout-Drubezki, Y. Gruenbaum, Dynamic interactions of nuclear lamina proteins with chromatin and transcriptional machinery, Cell. Mol. Life Sci. 60 (2003) 2053–2063, https://doi.org/10.1007/s00018-003-3038-3.
[24] C. Samson, A. Petitalot, F. Celli, I. Herrada, V. Ropars, M.H. Le Du, N. Nhiri, E. Jacquet, A.A. Arteni, B. Buendia, S. Zinn-Justin, Structural analysis of the ternary complex between lamin A/C, BAF and emerin identifies an interface disrupted in autosomal recessive progeroid diseases, Nucleic Acids Res. 46 (2018) 10460–10473, https://doi.org/10.1093/nar/gky736.
[25] Y. Turgay, O. Medalia, The structure of lamin filaments in somatic cells as revealed by cryo-electron tomography, Nucleus 8 (2017) 475–481, https://doi.org/10.1080/19491034.2017.1337622.
[26] S.J. Lee, Y.S. Jung, M.H. Yoon, S.M. Kang, A.Y. Oh, J.H. Lee, S.Y. Jun, T.G. Woo, H.Y. Chun, S.K. Kim, K.J. Chung, H.Y. Lee, K. Lee, G. Jin, M.K. Na, N.C. Ha, C. Barcena, J.M. Freije, C. Lopez-Otin, G.Y. Song, B.J. Park, Interruption of progerin-lamin A/C binding ameliorates Hutchinson-Gilford progeria syndrome phenotype, J. Clin. Invest. 126 (2016) 3879–3893, https://doi.org/10.1172/JCI84164.
[27] Z. Otwinowski, W. Minor, Processing of X-ray diffraction data collected in oscillation mode, Methods Enzymol. 276 (1997) 307–326.
[28] M.D. Winn, C.C. Ballard, K.D. Cowtan, E.J. Dodson, P. Emsley, P.R. Evans, R.M. Keegan, E.B. Krissinel, A.G. Leslie, A. McCoy, Overview of the CCP4 suite and current developments, Acta Crystallogr. Sect. D Biol. Crystallogr. 67 (2011) 235–242.
[29] J.J. Headd, N. Echols, P.V. Afonine, R.W. Grosse-Kunstleve, V.B. Chen, N.W. Moriarty, D.C. Richardson, J.S. Richardson, P.D. Adams, Use of knowledge-based restraints in phenix.refine to improve macromolecular refinement at low resolution, Acta Crystallogr. D Biol. Crystallogr. 68 (2012) 381–390, https://doi.org/10.1107/S0907444911047834.
[30] P.V. Afonine, R.W. Grosse-Kunstleve, N. Echols, J.J. Headd, N.W. Moriarty, M. Mustyakimov, T.C. Terwilliger, A. Urzhumtsev, P.H. Zwart, P.D. Adams, Towards automated crystallographic structure refinement with phenix.refine, Acta Crystallogr. Sect. D Biol. Crystallogr. 68 (2012) 352–367, https://doi.org/10.1107/S0907444912001308.
[31] P.V. Afonine, M. Mustyakimov, R.W. Grosse-Kunstleve, N.W. Moriarty, P. Langan, P.D. Adams, Joint X-ray and neutron refinement with phenix.refine, Acta Crystallogr. D Biol. Crystallogr. 66 (2010) 1153–1163, https://doi.org/10.1107/S0907444910026582.
[32] P. Emsley, K. Cowtan, Coot: model-building tools for molecular graphics, Acta Crystallogr. D Biol. Crystallogr. 60 (2004) 2126–2132, https://doi.org/10.1107/S0907444904019158.